





TnFLXopen: Markerless Transposons for Functional Fluorescent Fusion Proteins and Protein Interaction Prediction

 Felix Dempwolff,^{a,b}  Daniel B. Kearns^a

^aDepartment of Biology, Indiana University, Bloomington, Indiana, USA

^bCenter for Synthetic Microbiology (SYNMIKRO), Marburg, Germany

ABSTRACT Fluorescence microscopy of cells expressing proteins translationally linked to a fluorophore can be a powerful tool to investigate protein localization dynamics *in vivo*. One major obstacle to reliably analyze biologically relevant localization is the construction of a fusion protein that is both fluorescent and functional. Here, we develop a strategy to construct fluorescent fusions at theoretically any location in the protein by using TnFLXopen random transposon mutagenesis to randomly insert a gene encoding a fluorescent protein. Moreover, insertions within a target gene are enriched by an inducible gene-trap strategy and selection by fluorescence activated cell sorting. Using this approach, we isolate a variety of fluorescent fusions to FtsZ that exhibit ring-like localization and a fusion to the flagellar stator protein that both is functional for supporting motility and localizes as fluorescent puncta. Finally, we further modify TnFLXopen to insert the coding sequence for the C-terminal half of mVenus for use in bimolecular fluorescence complementation (BiFC) and the *in vivo* detection of protein-protein interaction candidates. As proof-of-concept, the DivIVA polar scaffolding protein was fused to the N terminus of mVenus, the C terminus of mVenus was delivered by transposition, and a combination of fluorescence activated cell sorter (FACS) sorting and whole-genome sequencing identified the known self-interaction of DivIVA as well as other possible candidate interactors. We suggest that the FACS selection is a viable alternative to antibiotic selection in transposon mutagenesis that can generate new fluorescent tools for *in vivo* protein characterization.

IMPORTANCE Transposon mutagenesis is a powerful tool for random mutagenesis, as insertion of a transposon and accompanying antibiotic resistance cassette often disrupt gene function. Here, we present a series of transposons with fluorescent protein genes which, when integrated in frame, may be selected with a fluorescence activated cell sorter (FACS). An open reading frame runs continuously through the transposon such that fluorescent protein fusions may be inserted theoretically anywhere in the primary sequence and potentially preserve function of the target protein. Finally, the transposons were further modified to randomly insert a partial fluorescent protein compatible with bimolecular fluorescence complementation (BiFC) to identify protein interaction candidates.

KEYWORDS *Bacillus subtilis*, BiFC, FACS, internal fluorescent protein fusion, protein-protein interactions, transposon mutagenesis, FtsZ, MotA, DivIVA

Transposons are mobile genetic elements that insert themselves into DNA and, as such, are powerful mutagens for forward genetic analysis. Each transposon is defined by two characteristic inverted terminal repeat (ITR) sequences and the DNA between them. A separate translocating enzyme, the transposase, recognizes and mobilizes the ITRs and intervening sequences to other locations in the chromosome (1, 2). Different transposases have different levels of insertion specificity, with some favoring particular locations while others are more random (3–6). The *mariner* transposase *Himar* exhibits almost no regional specificity, requiring only a TA-base doublet which is duplicated upon insertion of its cargo (7). The random insertion of transposons typically disrupts the function of the genes in which they

Editor Arpita Bose, Washington University in St. Louis

Copyright © 2022 Dempwolff and Kearns. This is an open-access article distributed under the terms of the [Creative Commons Attribution 4.0 International license](https://creativecommons.org/licenses/by/4.0/).

Address correspondence to Felix Dempwolff, dempwolff@uni-marburg.de, or Daniel B. Kearns, dbkearns@indiana.edu.

The authors declare no conflict of interest.

Received 2 December 2021

Accepted 8 April 2022

Published 2 May 2022

are inserted. When used in genetic screens, it is advantageous for the insertion frequency to be rare, as single insertions in the chromosome are preferable to multiple for the purposes of demonstrating linkage between the insertion and phenotype. Moreover, most transposons are engineered to encode a gene cassette conferring resistance to a particular antibiotic such that rare insertion events can be selected and the mutants subsequently screened.

While transposons are most commonly used for insertional mutagenesis, some systems have been deliberately reengineered to simultaneously introduce functional elements such as artificial outward-facing promoters that drive expression of genes adjacent to the insertion site or promoter-less genes for the generation of random reporter fusions (8–10). For example, a *mariner*-based transposon, TnFLX*gfp*, was developed by cloning a promoter-less *gfp* gene, encoding the green fluorescent protein (GFP), and encoding a downstream antibiotic resistance cassette between the two ITRs (11). Thus, a translational fusion between any theoretical target and GFP could be generated provided that the insertion placed the GFP coding sequence in frame. Translational fusions to GFP can be particularly advantageous as the magnitude of fluorescence indicates that gene expression level and subcellular localization patterns, if any, can be informative of gene function. Transposon-delivered reporter systems such as this, however, typically have two primary limitations for retaining function of the target. First, integration of a translational fusion often creates a C-terminal loss-of-function truncation of the target as translation is terminated by the reporter stop codon and downstream antibiotic resistance cassette necessary to select for colonies containing the insertion. Second, the location of the translational fusion is restricted to sites within an open reading frame permitted by the target transposase sequence and the single reading frame dictated by the ITR.

Here, we modify the *in vivo*-delivered TnFLX transposon system in *Bacillus subtilis* for the generation of internal markerless fusions to fluorescent protein reporters in all three open reading frames. While one of the constructs was nonfunctional due to unavoidable modification of the ITR, the remaining two exhibited transposition at frequencies sufficient for screening using a fluorescence activated cell sorter (FACS). We demonstrate the efficacy of the system by generating internal fluorescent fusions to the essential cell division protein FtsZ expressed in merodiploid at an ectopic site. We further show that the system can generate fusions that are both fluorescent and functional using the flagellar motor protein MotA as a nonessential target. Finally, we modify the transposon to deliver half of a fluorescent protein for random bimolecular fluorescence complementation (BiFC) screening of potential protein interactors with a target bait construct that is translationally coupled to the other half of the fluorophore in the chromosome (12–14). These tools will expand the ability to sample fluorescent fusion integration sites in proteins recalcitrant to reverse genetic fusion design and potentially provide a powerful new approach for unbiased screening of *in vivo* protein-protein interaction studies.

RESULTS

Development of transposons to create internal fluorescent protein fusions. To overcome the premature truncation of the target protein by the random integration of C-terminal translational fusions, a series of transposons were constructed which, when inserted into an expressed gene, would make in-frame, markerless fusions to the fluorescent protein mNeogreen. The transposons consisted of the *mNeogreen* open reading frame flanked by two inverted terminal repeats (ITRs) recognized by the *Himar* transposase (TnFLX*open*) (Fig. 1A). During transposition, the *Himar* transposase relocates the ITRs and intervening DNA into a randomly targeted TA-base doublet elsewhere in the genome (15, 16). If the TA integration site is located within a gene and cooriented with the target, then the transposon insertion could place the upstream ITR and the *mNeogreen* gene in one of three different reading frames. Moreover, during transposition, the TA target site is duplicated such that a TA repeat is found directly adjacent to both the upstream and downstream ITR and the 2-bp insertion would also perturb the open reading frame downstream of the transposon insertion site. Thus, three different transposon constructs were generated to accommodate the three different possible codon positions in which the TA target

bases were added to the 3' end of the *mNeongreen* gene to maintain the open reading frame (TnFLXopen3) (Fig. 1D).

To test the TnFLXopen*mNeongreen* series of transposons, a naturally competent derivative (DK1042) of the undomesticated *B. subtilis* wild-type strain NCIB 3610 (17) was separately transformed with each of the delivery plasmids. Transposon mutagenesis was conducted by propagating the resulting strains at a temperature permissive for plasmid replication (22°C), selecting for an antibiotic resistance cassette encoded in the plasmid backbone (*erm*), and back diluting the culture for regrowth in media lacking antibiotic at the nonpermissive temperature of 42°C. Note that transposition occurs at a constitutive rate and propagation at the nonpermissive temperature selects against extrachromosomal maintenance of the delivery vehicle to arrest transposon mobility. The resulting transposon libraries were subsequently analyzed by fluorescence microscopy. Cells lacking a transposon delivery system exhibited no fluorescence, but cells mutagenized with either TnFLXopen1 or TnFLXopen2 contained rare individuals that were fluorescent. Quantitation via flow cytometry allowed us to set a gate threshold based on the nonfluorescent wild type, and approximately 1:5,000 cells in a population mutagenized by TnFLXopen1 produced fluorescence above that threshold (Fig. 1E). The 10 variants of TnFLXopen3 were incapable of generating fluorescence detectable by microscopy, and flow cytometry indicated that even the best variant produced fluorescent cells at a frequency of perhaps 1:200,000. We infer that the reduced rate of transposition is likely attributed to the substantial genetic modification required to preserve the open reading frame, and due to the low frequency, TnFLXopen3 was dropped from further use. Nonetheless, the other two transposons integrated to create fluorescent fusion proteins at a frequency sufficient for screening even in the absence of antibiotic selection.

TnFLXopen*mNeongreen* internal fluorescent fusions to FtsZ. The absence of an antibiotic resistance cassette is advantageous as it permits the random generation of fluorescent fusions in the middle of a protein but is disadvantageous for targeted mutagenesis of a protein of interest. To circumvent this problem, a gene of interest whose gene product displays a distinct subcellular localization pattern was expressed from an IPTG (isopropyl- β -D-thiogalactopyranoside)-inducible *P_{hysp}* promoter and inserted at an ectopic locus (*amyE*) with a linked antibiotic resistance cassette. The candidate gene chosen was the *ftsZ* gene encoding the essential cell division protein FtsZ that localizes in a ring-like pattern at the cell division plane (18–21). The resulting strain was grown in the presence of IPTG and mutagenized in parallel with TnFLXopen1 and TnFLXopen2 to make random insertions, a subset of which generated fusions to FtsZ. To enrich for cells with FtsZ fusions, we first enriched for IPTG-induced cells expressing fluorescent proteins using a fluorescence activated cell sorter (FACS). The majority of cells mutagenized with the transposon exhibited low fluorescence intensity, but rare cells were fluorescent above a threshold and FACS sorting isolated these cells from the pool (Fig. 2A). The sorted population was then repropagated in the absence of IPTG and resorted by FACS, this time selecting for dark cells below the originally selected fluorescence intensity threshold (Fig. 2A). Thus, the probability that a fluorescent fusion was generated in *ftsZ* was increased by sequentially sorting the population for cells with fluorescence that was, like the expression of the *ftsZ* target, IPTG dependent.

To further determine linkage between the fluorescent fusion and the inducible copy of *ftsZ*, an SPP1 phage lysate was generated on the mutant pool and backcrossed by transduction into a wild-type parent selecting for the antibiotic resistance cassette integrated within the ectopic site. Some of the transductant colonies failed to exhibit fluorescence when induced with IPTG and were discarded. We attribute the absence of the enriched phenotype based on the fact that the FACS sorting protocol used was optimized for yield and not stringency and that depending on the nature of each insertion, cells may become nonfluorescent for reasons other than the lack of IPTG induction (e.g., heterogenous gene expression, transient dormancy, etc.). Nonetheless, other transductant colonies exhibited fluorescence upon IPTG induction. Some cells exhibited diffuse cytoplasmic fluorescence after induction, and all but one representative of this class was discarded (Fig. 2B). Sequencing indicated that the location of the transposon 57 bp downstream of the translational start site (FtsZ⁵⁷) would insert the mNeongreen protein sequence near the core of FtsZ structure, potentially

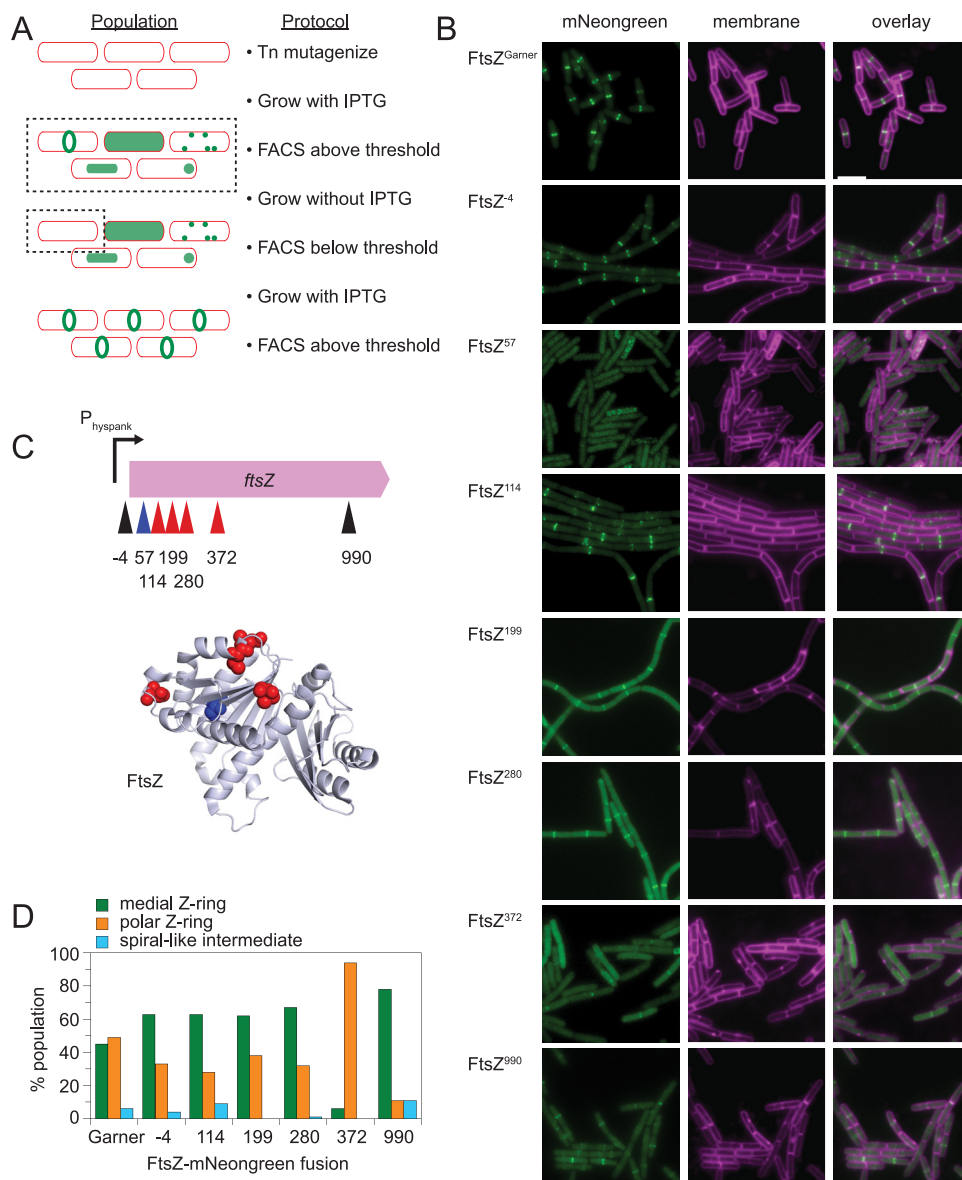


FIG 2 Some TnFLXopen insertions of mNeogreen within FtsZ produce subcellular fluorescence patterns consistent with FtsZ localization. (A) A flow diagram of the selection strategy used to enrich TnFLXopenmNeogreen insertions within *ftsZ*. Cells in a population are indicated by a red outline. After transposition, cells grown in the presence of IPTG were selected for fluorescence by FACS (dotted box), and the population exhibited a diverse variety of fluorescence localization patterns (green). The enriched population was regrown in the absence of IPTG, FACS sorted for nonfluorescent cells (dotted box), and plated. The resulting colonies were regrown in the presence of IPTG, colonies that produced fluorescent cells were retained, and the transposon insertion site within *ftsZ* was determined. (B) Fluorescence microscopy images of the indicated TnFLXopenmNeogreen insertions labeled with the corresponding insertion site. Membranes were stained with FM4-64 (false colored magenta) and FtsZ-mNeogreen (false colored green). The following strains were used to generate this panel: FtsZ^{Garner} (DK5094), FtsZ⁻⁴ (DK8445), FtsZ⁵⁷ (DK8441), FtsZ¹¹⁴ (DK8440), FtsZ¹⁹⁹ (DK8444), FtsZ²⁸⁰ (DK8443), FtsZ³⁷² (DK8439), and FtsZ⁹⁹⁰ (DK8442). (C) Top, location of transposon insertion sites within the *ftsZ* gene. Numbers indicate the distance (in bp) from the transposon insertion relative to the translation start site. Red carets indicate insertions predicted to position the mNeogreen fusion on the surface of the protein, blue caret indicates an insertion predicted to position mNeogreen in the FtsZ core region, and black carets indicate insertions that fall within unstructured domains not present in the FtsZ 3-dimensional structure. Bottom, ribbon diagram of the FtsZ protein (PDB 2VAM [60]) from *B. subtilis* with four of the mNeogreen insertion sites that led to distinct localization patterns space filled in red. Only diffuse localization was observed when insertion of the transposon led to fusion of mNeogreen to the internal core of the FtsZ protein (space filled in blue). AlphaFold2 was used to model each of the resulting fusion proteins (Fig. S2). Each fusion that gave rise to FtsZ-like localization patterns positioned mNeogreen such that it did not interfere with protofilament oligomerization, whereas the one fusion that abolished localization positioned mNeogreen in a steric clash with the adjacent monomer. (D) Localization analysis of cells expressing the various FtsZ-mNeogreen fusion proteins. Green bars represent percentage of events in which the FtsZ ring was observed at the predivisional midcell, orange bars indicate the percentage of events in which the FtsZ ring was observed adjacent to a nascent pole, and cyan bars indicate the percentage of events in which FtsZ adopted a spiral-like intermediate.

disrupting proper folding and producing the diffuse fluorescence observed (Fig. 2C). Fifteen transductants, however, exhibited a subcellular ring-like localization pattern reminiscent of the known pattern of FtsZ, and in each case the inducible copy of *ftsZ* was sequenced to determine the transposon insertion site. Nine of the candidates contained *mNeogreen* insertions that were redundant with others within the class consistent with the propagation of siblings during the enrichment process, and redundant insertions were discarded. Ultimately, six unique insertions in FtsZ were further characterized (Table S1, Fig. 2B). Two of the six were inserted in unresolved and likely disordered regions of the FtsZ protein structure, but the remaining four were inserted at surface-exposed sites perhaps consistent with partial functionality (Fig. 2C).

To determine whether any of the new mNeogreen-FtsZ insertions altered FtsZ localization, each FtsZ localization pattern was compared to a previously established N-terminal mNeogreen fusion to FtsZ, FtsZ^{Garner} (20). In *B. subtilis*, FtsZ has at least three different localization patterns. First, FtsZ localizes as a medial predivisional ring to recruit late divisome components (22–24). Second, after division is complete, the FtsZ ring dwells at the new polar position until disassembled by the Min system (25–27). Third, a subpopulation of FtsZ may migrate away from the polar ring toward the nascent midcell as a spiral-like intermediate (28, 29). In general, the TnFLXopen-delivered mNeogreen fusions exhibited higher background fluorescence than FtsZ^{Garner}, but this may be due to the fact that each of these constructs was expressed by IPTG induction from the artificial *P_{hyspank}* promoter in merodiploid whereas FtsZ^{Garner} is expressed in merodiploid from the native *ftsZ* promoter. While the higher background fluorescence in some cases reduced the ability to detect spirals, we note that four of the TnFLXopen fusions (FtsZ⁻⁴, FtsZ¹¹⁴, FtsZ¹⁹⁹, and FtsZ²⁸⁰) exhibited FtsZ localization position frequencies roughly similar to that exhibited by FtsZ^{Garner} (Fig. 2B). One fusion, however, FtsZ³⁷², appeared to exhibit preference for polar localization, while another, FtsZ⁹⁹⁰, exhibited preference for medial localization. We conclude that the location of the mNeogreen fusion within FtsZ can alter localization patterns. Moreover, the fusions that favor one ring location over another may inform FtsZ function, either by masking protein interaction sites or by altering the relative rates of protofilament polymerization/depolymerization.

A TnFLXopen fluorescent and functional fusion to MotA. Random fluorescent fusions were generated to FtsZ, but functionality was difficult to assess due to merodiploidy and the essential nature of the target. To screen for random fluorescent fusions that were also functional, a similar strategy was taken with a nonessential target, the flagellar stator proteins MotA and MotB (Fig. 3A) (30–33). A strain doubly mutated for *motA* and *motB* with an IPTG-inducible copy of the *motAmotB* dicistron at an ectopic site (*amyE*) exhibited swarming motility only in the presence of IPTG and was mutagenized with TnFLXopenmNeogreen (Fig. 3B, top). The transposon mutant pool was grown in the presence of IPTG, and FACS was used to select for the fluorescent subpopulation. Next, the subpopulation was regrown in the absence of IPTG and FACS selected for nonfluorescent cells to enrich for individuals in which fluorescence was, like *motAmotB* expression, IPTG dependent (Fig. 3A). Finally, the pool was regrown in the presence of IPTG and spotted in the center of an IPTG-containing swarm agar petri plate to measure motility. Transposants that were nonfunctional for MotA or MotB activity remained nonswarming at the site of inoculation. Cells emerged from the nonmotile population, however, and spread over the surface of the agar. Fifteen clonal isolates were selected by streaking from the swarm edge (Fig. 3B, top).

Microscopic analysis of the candidates grown in the presence of 1 mM IPTG revealed that cells exhibited diffuse fluorescence at the cell membrane with perhaps an indication of puncta within the haze (Fig. 3C). Fluorescent fusions to MotA and MotB in other organisms have exhibited a punctate localization pattern (34–38), and the diffuse staining of the membrane observed here may have been due to the overexpression of the *motAmotB* genes by the inducible promoter. Each candidate was sequenced to determine the location of the transposon insertion site and found to have the exact same insertion in which the *mNeogreen* gene was inserted upstream of, and in frame with, the *motA* gene, thereby generating an N-terminal fusion with a 12-amino acid-long linker sequence (Fig. 3D). Finally,

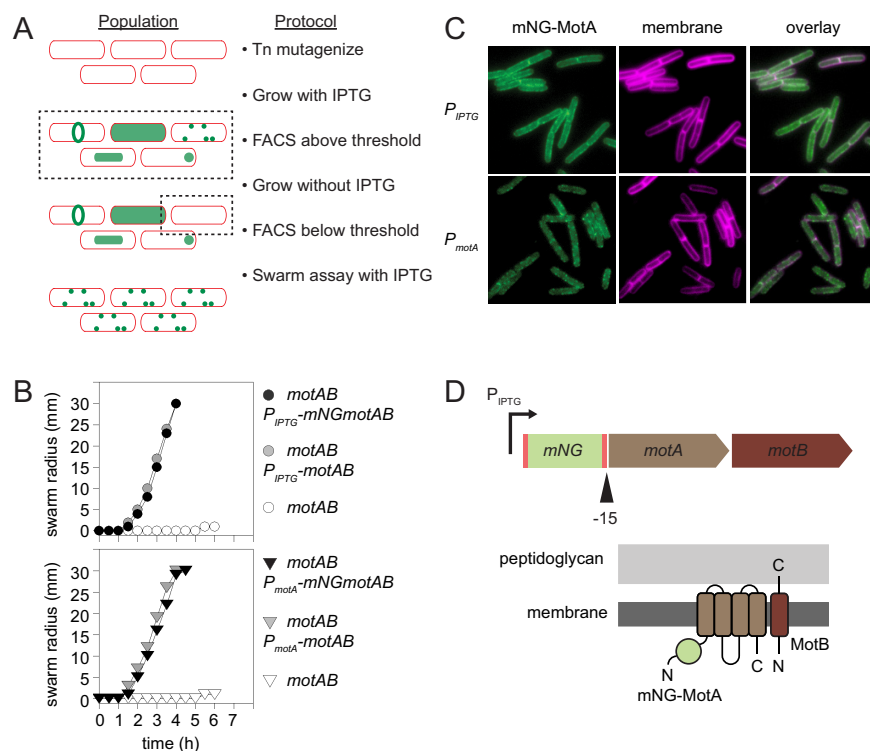


FIG 3 An mNeogreen-MotA fusion complements the lack of the wild-type *motA* gene. (A) A flow diagram of the selection strategy used to enrich *TnFLXopenmNeogreen* insertions within *motAB*. Cells in a population are indicated by a red outline. After transposition, cells grown in the presence of IPTG were selected for fluorescence by FACS (dotted box) and the population exhibited a diverse variety of fluorescence localization patterns (green). The enriched population was regrown in the absence of IPTG and FACS sorted for nonfluorescent cells (dotted box) and plated. The resulting colonies were regrown in the presence of IPTG, spotted on IPTG-containing swarm agar plates, and cells from motile flares were retained. (B) Quantitative swarm expansion assays. Top, the following strains were measured for motility on swarm agar plates in the presence of IPTG: *motAB* P_{IPTG} -*mNGmotAB* (open circles, DK2530), *motAB* P_{IPTG} -*motAB* (gray circles, DK801), *motAB* P_{IPTG} -*mNGmotAB* (closed circles, DK6666). Bottom, the following strains were measured for motility on swarm agar plates: *motAB* (open circles, DK2530), *motAB* P_{motA} -*motAB* (gray circles, DK8678), *motAB* P_{motA} -*mNGmotAB* (closed circles, DK7154). *mNG*, *mNeogreen*. Each data point is the average of three replicates. (C) Fluorescence microscopy images of the mNeogreen-MotA (mNG-MotA) fusion expressed from either the IPTG-inducible P_{IPTG} promoter (top, DK6832) or the native P_{motA} promoter (bottom, DK7104). Cell membrane was fluorescently stained with FM4-64 (false colored magenta) and mNG-MotA (false colored green). (D) Top, schematic representation of the *TnFLXopenmNeogreen* transposon inserted 15 bp upstream of the *MotA* translation start site. Bent arrow represents the IPTG-inducible promoter, red boxes represent inverted terminal repeat regions and the green box represents the *mNeonGreen* gene. Brown boxes represent the *motA* and *motB* genes, respectively, and the black caret indicates the location of the in-frame fusion event generated by transposon insertion. Bottom, model of the mNeogreen-MotA/MotB motor complex in the bacterial membrane. mNeogreen-MotA is represented in light brown with the fused mNeogreen highlighted as a green circle. MotB is colored in dark brown. Lipid bilayer is represented in dark gray, the cell wall in light gray. N and C indicate respective protein termini.

the N-terminal mNeogreen-MotA fusion was shown to complement the swarming motility defect of a *motAmotB* double mutant in the presence of IPTG (39) (Fig. 3B, top). We infer that either the single insertion represents the only functional insertion location within *motAmotB* or multiple functional insertion points are possible and the single recovered insertion was the result of sequential enrichment and propagation of siblings. Whatever the case, one candidate sibling was retained for further study.

To further characterize the mNeogreen-MotA fusion protein, the fusion-containing dicistron was cloned under the control of the native P_{motA} promoter and inserted at the ectopic *amyE* locus of a *motAmotB* *motAB* double mutant. Whereas strains deleted for the *motAB* operon have a mucoid colony morphology due to the overexpression of secreted poly- γ -glutamate (30, 31), the mNeogreen-MotA/MotB construct produced wild-type-looking colonies perhaps indicative of successful complementation. To quantitatively assess functionality of the P_{motA} -*mNeogreen-motAmotB* construct, a swarm expansion assay was performed and

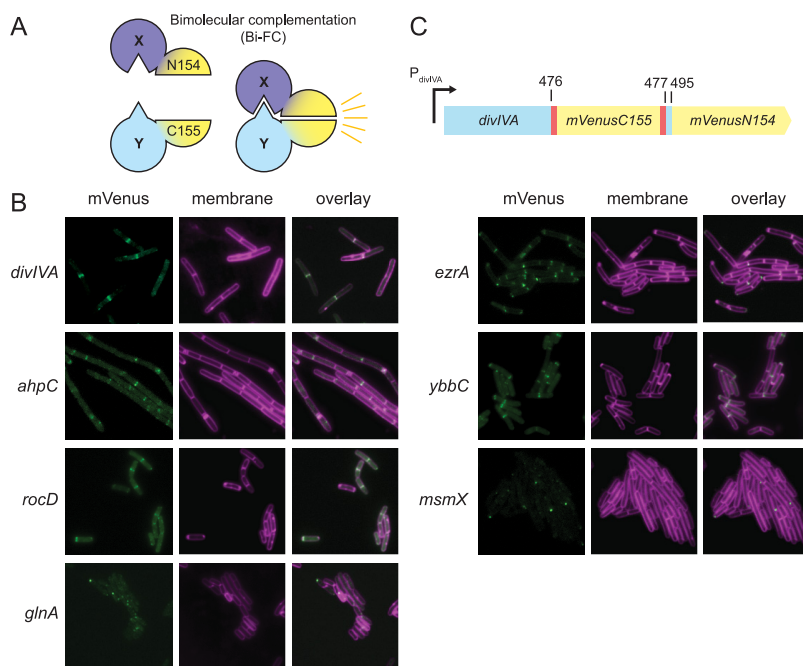


FIG 4 Transposon-delivered BiFC identified candidate DivIVA interactors. (A) Cartoon of bimolecular fluorescence complementation (BiFC) strategy. One half of a fluorophore mVenusN154 is fused to one protein of interest (protein X), and the other half of mVenusC155 is fused to another protein with which protein X interacts (protein Y). The interaction of proteins X and Y bring both mVenus halves into close spatial proximity, thereby restoring fluorophore structure and fluorescence emission. (B) Fluorescence micrographs of TnFLXopenmVenusC155 fusion candidates cloned under the control of an IPTG-inducible promoter and inserted at an ectopic locus of a strain expressing DivIVA-mVenusN154 at the native locus. Membrane stained with FM4-64 (false colored in magenta) and mVenus (false colored in green). The following strains were used to generate each panel: *ahpC* (DK8247), *divIVA* (DK8062), *ezrA* (DK8478), *glnA* (DK8179), *msmX* (DK8249), *rocD* (DK8479), and *ybbC* (DK8248). Bar represents 5 μm. (C) Cartoon of the TnFLXopenmVenusC155 fusion in the *divIVA-mVenusN154* reporter gene. The transposon inserted the C-terminal half of mVenus into the reporter upstream of the N-terminal half of mVenus. Blue box indicates *divIVA* sequence, yellow boxes indicate the mVenus sequence, and red boxes indicate the TnFLXopen Himar recognition ITR sequences. Numbers above the diagram indicate base pair locations. Bent arrow indicates the *divIVA* promoter.

the fusion protein was found to be functional as it rescued swarming of the *motAmotB* motAB mutant to wild-type levels (Fig. 3B, bottom). Finally, fluorescence microscopy of liquid-grown cells in exponential phase indicated that the mNeogreen-MotA fusion localized as puncta at the cell membrane consistent with MotA/MotB localization reported for other organisms (Fig. 3C). We conclude that the mNeogreen-MotA fusion is functional and fluorescent. We further conclude that transposon mutagenesis with TnFLXopenmNeogreen is a viable strategy for the unbiased generation and screening of random fusions that are both fluorescent and functional.

Transposon-mediated markerless fluorescent fusions for detecting protein interactions. Most proteins are a part of a cellular network, and their functions are frequently influenced by the proteins with which they interact. Therefore, the determination of proteins in close spatial proximity can help to understand the role of a protein in the cell. One method to detect protein interactions is bimolecular fluorescence complementation (BiFC) in which two halves of a fluorophore are fused to interacting proteins and the protein interaction restores fluorophore structure and function (12–14) (Fig. 4A). Here, we designed an unbiased approach to detect protein interactions using BiFC, random transposon mutagenesis, and high-throughput cell sorting by FACS. Briefly, a protein of interest, in this case the *B. subtilis* polar scaffolding protein DivIVA (40–43), was fused to the N-terminal 154 amino acids of the fluorophore mVenus (DivIVA-mVenus¹⁻¹⁵⁴) at the native site in the chromosome. The resulting strain was nonfluorescent due to the mVenus truncation. Next, the strain was mutagenized with derivatives of TnFLXopen in which sequences encoding the 84 C-terminal amino acids of mVenus were integrated between the mariner ITR sequences in the two functional reading

frames described previously (TnFLXopenmVenus^{C155}). Eight million cells from the transposon mutagenesis were FACS sorted for rare fluorescence, and 100 candidate colonies were recovered. We hypothesized that the transposons generated fusions to one or more proteins that interacted with DivIVA, such that their interaction brought the two domains of mVenus in spatial proximity and generated fluorescence.

Whole-genome sequencing was performed on seven of the fluorescent isolates to determine which transposon, sometimes among multiple, was fused in frame with a target gene candidate (Fig. S3). Each target in-frame fusion was PCR amplified and cloned under the control of an IPTG-inducible promoter to determine whether expression of that fusion alone was sufficient to restore fluorescence in the presence of DivIVA-mVenus^{N154}. Seven candidate insertions gave fluorescence upon induction (Fig. 4B). DivIVA dimerizes and forms interdimer contacts to create a polar scaffold-like mesh at the cell pole (44), and consistent with self-interaction, one of the BiFC transposon insertions landed within the DivIVA-mVenus^{N154} construct. The resulting fusion generated a protein in which the C-terminal and N-terminal fragments of mVenus switched order in the primary sequence (Fig. 4C). We infer that DivIVA oligomerization and/or subsequent supermolecular contacts within the mesh restored close proximity of the two fragments of mVenus, sufficient to generate fluorescence. Importantly, the insertion in DivIVA localized to both the nascent septum and the old pole, a pattern consistent with previously reported DivIVA localization (40). Four other transposon insertions in *ezaA* encoding the cell division regulator protein EzrA (45), *rocD* encoding the ornithine transaminase enzyme RocD (46), *ahpC* encoding the alkyl hydroperoxide reductase AhpC (47, 48), and *ybbC* encoding a protein of unknown function also produced fluorescence localization in a manner perhaps consistent with DivIVA (Fig. 4B). Two other insertions in *msmX* encoding the ABC-sugar transporter component MsmX (49) and *glnA* encoding glutamine synthetase GlnA (50) produced fluorescence puncta that were also typically found at the cell pole (Fig. 4B). We conclude that *in vivo*-delivered transposons carrying BiFC complementation fragments are capable of restoring fluorescence, thereby predicting candidate interaction proteins for a protein of interest.

DISCUSSION

Most translational fusions to fluorescent proteins are made at either the N or C terminus of a target protein for convenience, and such constructs are often sufficient to generate fusions that are both fluorescent and functional. Sometimes, however, N- and/or C-terminal fusions can disrupt or alter protein function, perhaps by interfering with proper folding, occluding protein interaction sites, or concealing regulatory domains like proteolytic degrons. When terminal fusions fail to preserve protein function, the generation of internal in-frame “sandwich” fusions can be advantageous, but the rational design of internal fusions is problematic, particularly when structural information for the protein of interest is absent (26, 51). Here, we modify a *mariner*-based transposon system for the generation of random fluorescent fusion proteins. Briefly, the system abandons the convention of including an antibiotic resistance cassette within the confines of the transposon and allows readthrough of a gene encoding a fluorescent protein when inserted in frame with a target gene in the genome. Instead of selecting for transposants based on growth in the presence of an antibiotic, fluorescence activated cell sorting (FACS) was used to select for fluorescent individuals. With this unbiased approach, the randomness of transposon insertion allows theoretically any location within a protein to be sampled for permissive sites of fusion that are fluorescent and/or functional to overcome the limitations of expectations and convenience (52).

While our transposon-based approach to fluorescent fusion protein generation has advantages, it also has weaknesses, as in the context of the entire genome, random transposon insertion makes recovering insertions in a particular gene of interest rare. Here, we overcome this limitation by a “trap” strategy in which a gene of interest is inserted in the chromosome under the control of an inducible promoter, adjacent to a preexistent antibiotic resistance cassette. Thus, linkage of the fluorescent fusion to the gene of interest can be established by a combination of IPTG-dependent fluorescence and linkage to the preexistent antibiotic resistance. The trap-based approach allowed isolation of a number of insertions in

FtsZ that produced localization patterns consistent with FtsZ rings previously established by both fluorescent fusions and immunolocalization. Moreover, a single mNeogreen fusion was recovered for the MotA flagellar stator protein that not only gave a membrane-associated, punctate localization pattern consistent with tagged homologs in other organisms but was also functional for supporting motility when present as the only copy. We conclude that the TnFLXopen system combined with a genetic trap can permit selective retrieval of fluorescent and/or functional fusions to theoretically any protein of interest.

We further expanded the TnFLXopen system for the detection of protein-protein interactions *in vivo* by bimolecular complementation of fluorescence (BiFC). Specifically, half of a fluorophore was fused to a protein of interest and the other half was delivered by transposon insertion. If the insertion generated an in-frame fusion to an interacting partner, the two halves of the fluorophore were brought into functional proximity and that individual clone could be retrieved by FACS. Linkage analysis was problematic due to the absence of an antibiotic resistance cassette linked to the complementary construct, but whole-genome sequencing was sufficient to identify in-frame candidates that could be recloned and tested in isolation. The BiFC system was successful in recovering a known interactor with the polar scaffolding protein DivIVA, namely, DivIVA itself. The approach seemed susceptible to perhaps false-positive interactions with highly abundant metabolic proteins but also yielded other potentially relevant interacting proteins like the cell division regulator EzrA. We conclude that transposon-delivered BiFC was successful at identifying interacting partners with a protein of interest and provides an unbiased *in vivo* approach to protein-protein interaction studies. Moreover, BiFC provides additional protein interaction information at the subcellular level.

Here, we describe a number of applications and strategies for the use of markerless transposons for the generation of random fluorescent protein fusions, but we expect that many other permutations are possible. For example, we imagine that *in vitro* delivery could be used as an alternative to the *in vivo* system, high-throughput microscopic screening of individual colonies could replace FACS analysis, and introduction of a cassette linked to a native gene could serve as a trap for native fluorescent fusion insertion. Whatever the modification, these approaches are not intended to replace rational design, particularly those now aided by protein folding programs, but instead serve as a potentially valuable alternative when such approaches fail, as was the case in generating fusions to the *B. subtilis* flagellar stator protein complex. Moreover, the tools can be used beyond targeted gene insertion for whole-genome screens such as we demonstrate here by the transposon-delivered BiFC approach for predicting protein interactions. Finally, we anticipate that these tools will be useful in their own right but also spark interest and inspiration in broadening of transposon insertion selections beyond the use of traditional antibiotic resistance cassettes.

MATERIALS AND METHODS

Strains and growth conditions. All strains used in the study are listed in Table 1.

B. subtilis and *Escherichia coli* strains were grown in lysogeny broth (LB; 10 g tryptone, 5 g yeast extract, 5 g NaCl per L) or on LB plates fortified with 1.5% (wt/vol) Bacto agar at 37°C. When appropriate, antibiotics were included at the following concentrations: 10 µg/mL tetracycline, 100 µg/mL spectinomycin, 5 µg/mL chloramphenicol, 5 µg/mL kanamycin, and 1 µg/mL erythromycin plus 25 µg/mL lincomycin (*mIs*). Isopropyl-β-D-thiogalactopyranoside (IPTG; Sigma-Aldrich, St. Louis, USA) was added to the medium at the indicated concentration when appropriate.

Strain creation and maintenance. All plasmids used in the study are listed in Table S2. All primers used in the study are listed in Table S3. For the construction of the transposon delivery vectors, plasmids were amplified in *E. coli* DH5α and transferred to *E. coli* TG1 (*recA*⁺) to generate plasmid concatemers and allow for transformation into *B. subtilis*.

Construction of the TnFLXopen delivery plasmids. To generate TnFLXopen1mNeogreen, the *mNeogreen* gene was equipped with flanking ITRs and a 1-bp spacer distal to the region coding for the fluorophore to maintain the proper reading frame by PCR using chromosomal DNA of DK3394 as a template and oligonucleotides 5680 and 5681. To allow for integration into the universal transposon acceptor plasmid pFK7 (11) at an SmaI restriction site, the obtained fragment was amplified and extended with primers 5759 and 5760 and isothermal assembly (ITA) was performed yielding pFK169 (see Fig. S4 for plasmid sequence).

To generate TnFLXopen2mNeogreen, the *mNeogreen* gene was equipped with flanking ITRs as well as 2-bp spacers proximal and distal to the coding region to maintain the proper reading frame by PCR using chromosomal DNA of DK3394 as a template and oligonucleotides 6949 and 6950. To allow for integration into the universal transposon acceptor plasmid pFK7 at an SmaI restriction site, the obtained

TABLE 1 Strains

Strain	Genotype	Tn tag ^a
DK1042	<i>comJ</i> ^{O12L} wild type (17)	
PY79	<i>sfp</i> ⁰ <i>swrA</i> ^{ES} (61)	
DK801	<i>motAB::tet amyE::P_{hyspank}-motAB spec</i> (62)	
DK2530	<i>motAB::tet</i>	
DK3394	<i>amyE::P_{hyspank}-mNeongreen spec</i>	
DK5094	<i>mNeongreen-FtsZ^{Gamer}</i>	
DK6008	Ω <i>divIVA-mVenusN154 cat rocD::TnFLXopenmVenusC155</i>	TATGCAAGGA
DK6012	Ω <i>divIVA-mVenusN154 cat divIVA::TnFLXopenmVenusC155</i>	TATTTGAGGA
DK6013	Ω <i>divIVA-mVenusN154 cat ahpC::TnFLXopenmVenusC155</i>	TATGCCAAC
DK6035	Ω <i>divIVA-mVenusN154 cat ybbC::TnFLXopenmVenusC155</i>	TAGAACCTGA
DK6630	Ω <i>divIVA-mVenusN154 cat</i>	
DK6666	<i>motAB::tet amyE::P_{hyspank}-TnFLXopenmNeongreen-motAB spec</i>	
DK6832	<i>motAB::tet amyE::P_{hyspank}-motAB::TnFLXopenmNeongreen spec</i>	TAGACAAGCT
DK6833	<i>motAB::tet amyE::P_{hyspank}-motAB::TnFLXopenmNeongreen spec</i>	TAGACAAGCT
DK7154	<i>motAB::tet amyE::P_{motA}-mNeongreen-MotAB spec</i>	
DK7191	Ω <i>divIVA-mVenusN154 cat ezrA::TnFLXopenmVenusC155</i>	TAGATGATGT
DK7196	Ω <i>divIVA-mVenusN154 cat msmX::TnFLXopenmVenusC155</i>	TACATGATGA
DK7197	Ω <i>divIVA-mVenusN154 cat glnA::TnFLXopenmVenusC155</i>	TAGCATGGAG
DK8062	<i>amyE::P_{hyspank}-divIVA-mVenusN154::TnFLXmVenusC155 cat</i>	TATTTGAGGA
DK8158	<i>amyE::P_{hyspank} ftsZ kan</i>	
DK8179	Ω <i>divIVA-mVenusN154 cat amyE::P_{hyspank} glnA::TnFLXmVenusC155 cat</i>	TAGCATGGAG
DK8247	Ω <i>divIVA-mVenusN154 cat amyE::P_{hyspank} ahpC::TnFLXmVenusC155 cat</i>	TATGCCAAC
DK8248	Ω <i>divIVA-mVenusN154 cat amyE::P_{hyspank} ybbC::TnFLXmVenusC155 cat</i>	TAGAACCTGA
DK8249	Ω <i>divIVA-mVenusN154 cat amyE::P_{hyspank} msmX::TnFLXmVenusC155 cat</i>	TACATGATGA
DK8439	<i>amyE::P_{hyspank} ftsZ³⁷²TnFLXopenmNeongreen kan</i>	TAGGCGCATT
DK8440	<i>amyE::P_{hyspank} ftsZ¹¹⁴TnFLXopenmNeongreen kan</i>	TAGAGTATAT
DK8441	<i>amyE::P_{hyspank} ftsZ⁵⁷TnFLXopenmNeongreen kan</i>	TAGGAGGCGG
DK8442	<i>amyE::P_{hyspank} ftsZ⁹⁹⁰TnFLXopenmNeongreen kan</i>	TAAATCAAAG
DK8443	<i>amyE::P_{hyspank} ftsZ²⁸⁰TnFLXopenmNeongreen kan</i>	TAAAGGTGCT
DK8444	<i>amyE::P_{hyspank} ftsZ¹⁹⁹TnFLXopenmNeongreen kan</i>	TAGAGGATTG
DK8445	<i>amyE::P_{hyspank} ftsZ⁻⁴TnFLXopenmNeongreen kan</i>	TAGAATGTTG
DK8478	Ω <i>divIVA-mVenusN154 cat amyE::P_{hyspank} ezrA::TnFLXmVenusC155 cat</i>	TAGATGATGT
DK8479	Ω <i>divIVA-mVenusN154 cat amyE::P_{hyspank} rocD::TnFLXmVenusC155 cat</i>	TATGCAAGGA
DK8580	Ω <i>divIVA-mVenusN154 cat citB::TnFLXopenmVenusC155</i>	TATTGATGTT
DK8678	<i>motAB::tet amyE::P_{motA}-TnFLXopenmNeongreen-motAB spec</i>	

^aTn tag indicates the nine base pairs adjacent to the transposon insertion site to allow precise determination of transposon position.

fragment was amplified and extended with primers 5759 and 5760 and isothermal assembly was performed creating pFK87 (see Fig. S4 for plasmid sequence).

To generate TnFLXopen1mVenusC155, the last 255 bp of the coding region of the *mVenus* gene (*mVenus C155*) was extended with ITRs and a 1-bp spacer distal to the gene fragment to maintain the proper reading frame by PCR amplification using an *mVenus* linear fragment optimized for the codon usage of *B. subtilis* (synthesized by IDT, Coralville, IA) and oligonucleotides 6146 and 6147. The resulting transposon was re-PCR amplified using primers 5759 and 5760, purified, and integrated into SmaI linearized pFK7 by ITA to create plasmid pFK170 (see Fig. S4 for plasmid sequence).

To generate TnFLXopen2mVenusC155, *mVenusC155* was PCR amplified with oligonucleotides 6953 and 6954, which introduced flanking ITR sequences and two base pair spacers proximal and distal to the gene fragment to maintain reading frame integrity. The resulting transposon was re-PCR amplified using primers 5759 and 5760, purified, and integrated into SmaI linearized pFK7 by ITA to create plasmid pFK110 (see Fig. S4 for plasmid sequence).

DivIVA-mVenusN154. A fusion between a truncated *divIVA* gene and the proximal 462 bp of the *mVenus* gene was generated by ITA (53). The *divIVA* fragment was PCR amplified from DK1042 chromosomal DNA using oligonucleotides 6150 and 6151, and the *mVenus* fragment was PCR amplified from a fragment optimized for the codon usage of *B. subtilis* (synthesized by IDT, Coralville, IA) using oligonucleotides 6152 and 6153 and cloned by ITA into pER19 (54) linearized by SmaI digestion to make pFK86. The pFK86 was isolated from *recA*⁺ TG1 *E. coli* and transformed into DK1042, yielding DK6630.

***P_{motA}*-mNeongreen-motAmotB.** The *P_{motA}*-mNeongreen-motAmotB construct was assembled by amplification of the *P_{motA}* sequence with the oligonucleotides 6722 and 6723 using chromosomal DNA of DK1042 as the template and the *mNeongreen-motAmotB* fragment with the oligonucleotides 6724 and 6725 and chromosomal DNA of DK6832. The fragments were restriction-digested with BamHI/Sall and Sall/SphI, respectively, and inserted into BamHI/SphI linearized pAH25 (generous gift of Amy Hitchcock Camp, Mount Holyoke College) by ligation, creating pDP530.

ITPG-inducible constructs. The *ftsZ* gene was PCR amplified using DK1042 chromosomal DNA as a template and oligonucleotides 7345 and 7346, purified, and integrated by ITA into pDP111 containing

the P_{hyspank} promoter, a polylinker, and a kanamycin resistance cassette between the arms of the *amyE* genes linearized by SphI to create pFK214 (55). The *ahpC-mVenusC155* gene was PCR amplified using DK6013 chromosomal DNA as a template and oligonucleotides 7365/7366 and integrated by ITA into Sall linearized pDP111 to create pFK222. The *divIVA-mVenusC155-mVenusN154* was PCR amplified using DK6012 chromosomal DNA and with oligonucleotides 7353/7354 and integrated by ITA into Sall linearized pDP111 to create pFK220. The *eziA-mVenusC155* gene was PCR amplified using DK7191 chromosomal DNA and oligonucleotides 7355/7356 and integrated by ITA into Sall linearized pDP111 to create pFK231. The *glnA-mVenusC155* gene was PCR amplified using DK7197 chromosomal DNA and oligonucleotides 7357/7358 and integrated by ITA into Sall linearized pDP111 to create pFK225. The *msmX-mVenusC155* gene was PCR amplified using DK7196 chromosomal DNA and oligonucleotides 7251/7352 and integrated by ITA into Sall linearized pDP111 to create pFK226. The *rocD-mVenusC155* gene was PCR amplified using DK6008 chromosomal DNA and oligonucleotides 7394/7395 and integrated by ITA into Sall linearized pDP111 to create pFK233. The *ybcC-mVenusC155* gene was PCR amplified using DK6035 chromosomal DNA and oligonucleotides 7361/7362 and integrated by ITA into Sall linearized pDP111 to create pFK223.

Isothermal assembly reaction. First, a 5× ITA stock mixture was generated (500 mM Tris-HCl [pH 7.5], 50 mM MgCl₂, 50 mM dithiothreitol [DTT; Bio-Rad, Hercules, CA, USA], 31.25 mM PEG-8000 [Thermo Fisher Scientific, Waltham, MA, USA], 5.02 mM NAD [Sigma-Aldrich], and 1 mM each deoxynucleoside triphosphate [dNTP; New England BioLabs, Ipswich, USA]), aliquoted, and stored at −80°C. An assembly master mixture was made by combining prepared 5× isothermal assembly reaction buffer (131 mM Tris-HCl, 13.1 mM MgCl₂, 13.1 mM DTT, 8.21 mM PEG-8000, 1.32 mM NAD, and 0.26 mM each dNTP) with Phusion DNA polymerase (New England BioLabs; 0.033 units/μL), T5 exonuclease diluted 1:5 with 5× reaction buffer (New England BioLabs; 0.01 units/μL), *Taq* DNA ligase (New England BioLabs; 5,328 units/μL), and additional dNTPs (267 μM). The master mix was aliquoted as 15 μL and stored at −80°C. DNA fragments were combined at equimolar amounts to a total volume of 5 μL and added to a 15-μL aliquot of prepared master mix. The reaction mixture was incubated for 60 min at 50°C (53).

Transposon mutagenesis. The transposon-harboring plasmids were introduced into the *B. subtilis* acceptor strain via transformation or SP1 phage-mediated transduction (56), selecting for *mls* resistance, and incubated at 22°C for 72 h. Subsequently, cells were incubated for 16 h (*TnFLXopenmNeongreen*) or 30 h (*TnFLXopenmVenusC155*) at room temperature in LB medium containing *mls*. The longer one incubates cells carrying the delivery plasmid, the more transposition events will occur, and we found that obtaining rare positive BiFC events benefited from longer incubations. After incubation, the cell suspension was diluted 1:100 in LB medium and grown for 6 h at 37°C to cure the cells of the plasmid. Subsequently, the cells were either screened by FACS or inoculated on LB-agar plates.

Whole-genome sequencing. Cells were grown in LB medium at 37°C to mid-exponential phase (optical density at 600 nm [OD₆₀₀] of ~0.5) and harvested, and genomic DNA was extracted with the DNeasy blood and tissue kit (Qiagen, Hilden, Germany). Illumina sequencing was performed by the Microbial Genome Sequencing Center (Pittsburgh, PA, USA).

Transposon insertion site identification by IPCR. Transposon insertions in the manuscript were identified either by sequencing a known locus or by unbiased whole-genome sequencing. Nonetheless, we developed a system for inverse PCR (IPCR) should one require such a protocol. Cells were grown in LB medium at 37°C for 6 h. DNA was isolated, and 6 μg was digested with 2 U/μg DNA of the restriction endonuclease *Sau3AI* (New England Biolabs). Ligation with 400 U of T4 DNA ligase (NEB) was performed at room temperature for 2 h with 1.5 μg of the digested DNA. Inverse PCR was performed with 6 μL of ligated DNA using the oligonucleotides 6987 and 6988 for the *TnFLXopenmNeongreen*, or 6118 and 6119 for the *TnFLXmVenusC155* system, respectively. The amplified fragment was analyzed by Sanger sequencing (Eurofins Genomics, Louisville, KY, USA) using the oligonucleotide 6987 (*TnFLXopenmNeongreen*) or 6118 (*TnFLXmVenusC155*).

Fluorescence microscopy. Microscopy was performed with a Nikon eclipse 80i microscope, equipped with a Plan Apo 100× Ph 3 objective (NA 1.4). Cells were mounted on 1% (wt/vol) agarose pads containing S7₅₀ minimal medium (57) on object slides. Images were acquired with a Cool snap HQ2 camera (Photometrix) and were processed with Metamorph 7.7.9 software (Universal Imaging Corp.). Membranes were stained with FM4-64 (1 nM final concentration, Molecular Probes).

Flow cytometry. Cells were grown in LB medium at 37°C to an OD₆₀₀ of 0.7, sedimented, and resuspended in phosphate-buffered saline (PBS; 137 mM NaCl, 2.7 mM KCl, 10 mM Na₂HPO₄, and 2 mM KH₂PO₄) at a concentration of 5 × 10⁶ cells/mL. Analysis and cell sorting were performed using a FACSArial flow cytometer (BD Biosciences, IUB Flow Cytometry Core Facility) equipped with an 85-μm nozzle. Cells that were separated by FACS were collected in a reaction tube containing LB medium and transferred onto fortified medium for further incubation.

Swarm expansion assay. Cells were grown in LB medium to mid-exponential phase at 37°C, sedimented, and resuspended to an OD₆₀₀ of 10 in water supplemented with 0.5% (vol/vol) India ink. Ten microliters of the cell suspension was spotted onto solidified LB agar (0.7% [wt/vol], freshly prepared, and dried for 10 min in a laminar flow hood), dried for 10 min, and incubated at 37°C. Measurements of swarm radius relative to the point of inoculation (demarcated by the India ink) were taken every 30 min. IPTG was supplemented to the medium at a concentration of 1 mM when appropriate.

Protein structure modeling. Three-dimensional structures were modeled using the ColabFold (58) software, which is based on the structure prediction provided by alphaFold2 (59). The structures were predicted using the following parameters: “Amber” = yes, “templates” = yes, “msa mode” = MMseqs2 (UniRef + Environmental), “model type” = auto, “pair mode” = unpaired + paired, “recycles” = 3.

Data availability. All data generated or analyzed during this study are included in this article. Raw data and bacterial strains can be requested from the corresponding authors. Relevant plasmids will be deposited at the Bacillus Genetic Stock Center (BGSC, The Ohio State University, Columbus OH).

SUPPLEMENTAL MATERIAL

Supplemental material is available online only.

SUPPLEMENTAL FILE 1, PDF file, 0.8 MB.

ACKNOWLEDGMENTS

We thank Christiane Hassel, Manager of the IUB Flow Cytometry Core Facility, Kate Hummels, Erhard Bremer (Marburg University, Germany), and Sandra Sanchez for technical support and helpful discussion. This work was funded by National Institutes of Health R35 grant GM131783 and grant R01 GM113172 to D.B.K.

REFERENCES

- Kleckner N. 1981. Transposable elements in prokaryotes. *Annu Rev Genet* 15:341–404. <https://doi.org/10.1146/annurev.ge.15.1.20181.002013>.
- Kleckner N. 1990. Regulation of transposition in bacteria. *Annu Rev Cell Biol* 6:297–327. <https://doi.org/10.1146/annurev.cb.06.110190.001501>.
- Harshey RM. 2014. Transposable phage *Mu*. *Microbiol Spectr* 2. <https://doi.org/10.1128/microbiolspec.MDNA3-0007-2014>.
- Peters JE. 2014. Tn7. *Microbiol Spectr* 2. <https://doi.org/10.1128/microbiolspec.MDNA3-0010-2014>.
- Nicolas E, Lambin M, Dandoy D, Galloy C, Nguyen N, Oger CA, Hallet B. 2015. The Tn3-family of replicative transposons. *Microbiol Spectr* 3. <https://doi.org/10.1128/microbiolspec.MDNA3-0060-2014>.
- Haniford DB, Ellis MJ. 2015. Transposons Tn70 and Tn5. *Microbiol Spectr* 3:MDNA3-0002-2014. <https://doi.org/10.1128/microbiolspec.MDNA3-0002-2014>.
- Tellier M, Claeys Bouuaert C, Chalmers R. 2015. Mariner and the ITm superfamily of transposons. *Microbiol Spectr* 3:MDNA3-0033-2014. <https://doi.org/10.1128/microbiolspec.MDNA3-0033-2014>.
- Perkins JB, Youngman PJ. 1986. Construction and properties of Tn917-*lac*, a transposon derivative that mediates transcriptional gene fusions in *Bacillus subtilis*. *Proc Natl Acad Sci U S A* 83:435–445.
- Zagorec M, Steinmetz M. 1991. Construction of a derivative of Tn917 containing an outward-directed promoter and its use in *Bacillus subtilis*. *J Gen Microbiol* 137:107–112. <https://doi.org/10.1099/00221287-137-1-107>.
- Pozsgai ER, Blair KM, Kearns DB. 2012. Modified mariner transposons for random inducible-expression insertions and transcriptional reporter fusion insertions in *Bacillus subtilis*. *Appl Environ Microbiol* 78:778–785. <https://doi.org/10.1128/AEM.07098-11>.
- Dempwolff F, Sanchez S, Kearns DB. 2020. TnFLX, a third generation mariner-based transposon system for *Bacillus subtilis*. *Appl Environ Microbiol* 86:e02893-19. <https://doi.org/10.1128/AEM.02893-19>.
- Ghosh I, Hamilton AD, Regan L. 2000. Antiparallel leucine zipper-directed protein reassembly: application to the green fluorescent protein. *J Am Chem Soc* 122:5658–5659. <https://doi.org/10.1021/ja994421w>.
- Hu CD, Kerppola TK. 2003. Simultaneous visualization of multiple protein interactions in living cells using multicolor fluorescence complementation analysis. *Nat Biotechnol* 21:539–545. <https://doi.org/10.1038/nbt816>.
- Kerppola TK. 2008. Bimolecular fluorescence complementation (BiFC) analysis as a probe of protein interactions in living cells. *Annu Rev Biophys* 37:465–487. <https://doi.org/10.1146/annurev.biophys.37.032807.125842>.
- Lampe DJ, Grant TE, Robertson HM. 1998. Factors affecting transposition of the *Himar1* mariner transposon *in vitro*. *Genetics* 149:179–187. <https://doi.org/10.1093/genetics/149.1.179>.
- Perry BJ, Yost CK. 2014. Construction of a mariner-based transposon vector for use in insertion sequence mutagenesis in selected members of the *Rhizobiales*. *BMC Microbiol* 14:298. <https://doi.org/10.1186/s12866-014-0298-z>.
- Konkol MA, Blair KM, Kearns DB. 2013. Plasmid-encoded ComI inhibits competence in the ancestral 3610 strain of *Bacillus subtilis*. *J Bacteriol* 195:4085–4093. <https://doi.org/10.1128/JB.00696-13>.
- Bi E, Lutkenhaus J. 1991. FtsZ ring structure associated with division in *Escherichia coli*. *Nature* 354:161–164. <https://doi.org/10.1038/354161a0>.
- Ma X, Ehrhardt DW, Margolin W. 1996. Colocalization of cell division proteins FtsZ and FtsA to cytoskeletal structures in living *Escherichia coli* cells by using green fluorescent protein. *Proc Natl Acad Sci U S A* 93:12998–13003. <https://doi.org/10.1073/pnas.93.23.12998>.
- Bisson-Filho AW, Hsu Y-P, Squyres GR, Kuru E, Wu F, Jukes C, Sun Y, Dekker C, Holden S, VanNieuwenhze MS, Brun YV, Garner EC. 2017. Treadmilling by FtsZ filaments drives peptidoglycan synthesis and bacterial cell division. *Science* 355:739–743. <https://doi.org/10.1126/science.aak9973>.
- Yang X, Lyu Z, Miguel A, McQuillen R, Huang KC, Xiao J. 2017. GTPase activity-coupled treadmill of the bacterial tubulin FtsZ organizes septal cell wall synthesis. *Science* 355:744–747. <https://doi.org/10.1126/science.aak9995>.
- Levin PA, Losick R. 1996. Transcription factor Spo0A switches the localization of the cell division protein FtsZ from a medial to bipolar pattern in *Bacillus subtilis*. *Genes Dev* 10:478–488. <https://doi.org/10.1101/gad.10.4.478>.
- Goehring NW, Gueiros-Filho F, Beckwith J. 2005. Premature targeting of a cell division protein to midcell allows dissection of divisome assembly in *Escherichia coli*. *Genes Dev* 19:127–137. <https://doi.org/10.1101/gad.1253805>.
- Gamba P, Veening J-W, Saunders NJ, Hamoen LW, Daniel RA. 2009. Two-step assembly dynamics of the *Bacillus subtilis* divisome. *J Bacteriol* 191:4186–4194. <https://doi.org/10.1128/JB.01758-08>.
- Levin PA, Shim JJ, Grossman AD. 1998. Effect of *minCD* on FtsZ ring position and polar septation in *Bacillus subtilis*. *J Bacteriol* 180:6048–6051. <https://doi.org/10.1128/JB.180.22.6048-6051.1998>.
- Gregory JA, Becker EC, Pogliano K. 2008. *Bacillus subtilis* MinC destabilizes FtsZ-rings at new cell poles and contributes to the timing of cell division. *Genes Dev* 22:3475–3488. <https://doi.org/10.1101/gad.1732408>.
- Yu Y, Zhou J, Dempwolff F, Baker JD, Kearns DB, Jacobson SC. 2020. The Min system disassembles FtsZ foci and inhibits polar peptidoglycan remodeling in *Bacillus subtilis*. *mBio* 11:e03197-19. <https://doi.org/10.1128/mBio.03197-19>.
- Wu LJ, Errington J. 2004. Coordination of cell division and chromosome segregation by a nucleoid occlusion protein in *Bacillus subtilis*. *Cell* 117:915–925. <https://doi.org/10.1016/j.cell.2004.06.002>.
- Yu Y, Zhou J, Gueiros-Filho FJ, Kearns DB, Jacobson SC. 2021. Noc corrals migration of FtsZ protofilaments during cytokinesis in *Bacillus subtilis*. *mBio* 12:e02964-20. <https://doi.org/10.1128/mBio.02964-20>.
- Cairns LS, Marlow VL, Bissett E, Ostrowski A, Stanley-Wall NR. 2013. A mechanical signal transmitted by the flagellum controls signaling in *Bacillus subtilis*. *Mol Microbiol* 90:6–21. <https://doi.org/10.1111/mmi.12342>.
- Chan JM, Guttenplan SB, Kearns DB. 2014. Defects in the flagellar motor increase synthesis of poly-g-glutamate in *Bacillus subtilis*. *J Bacteriol* 196:740–753. <https://doi.org/10.1128/JB.01217-13>.
- Deme JC, Johnson S, Vickery O, Aron A, Monkhouse H, Griffiths T, James RH, Berks BC, Coulton JW, Stansfeld PJ, Lea SM. 2020. Structures of the stator complex that drives rotation of the bacterial flagellum. *Nat Microbiol* 5:1553–1564. <https://doi.org/10.1038/s41564-020-0788-8>.
- Santiveri M, Roa-Eguia A, Kühne C, Wadhwa N, Hu H, Berg HC, Erhardt M, Taylor NMI. 2020. Structure and function of stator units of the bacterial flagellar motor. *Cell* 183:244–257. <https://doi.org/10.1016/j.cell.2020.08.016>.
- Leake MC, Chandler JH, Wadhams GW, Bai F, Berry RM, Armitage JP. 2006. Stoichiometry and turnover in single, functioning membrane protein complexes. *Nature* 443:355–358. <https://doi.org/10.1038/nature05135>.
- Paulick A, Koerdet A, Lassak J, Huntley S, Wilms I, Narberhaus F, Thormann KM. 2009. Two different stator systems drive a single polar flagellum in *Shewanella oneidensis* MR-1. *Mol Microbiol* 71:836–850. <https://doi.org/10.1111/j.1365-2958.2008.06570.x>.
- Lele PP, Hosu BG, Berg HC. 2013. Dynamics of mechanosensing in the bacterial flagellar motor. *Proc Natl Acad Sci U S A* 110:11839–11844. <https://doi.org/10.1073/pnas.1305885110>.
- Tippling MJ, Delalez NJ, Lim R, Berry RM, Armitage JP. 2013. Load-dependent assembly of the bacterial flagellar motor. *mBio* 4:e00551-13. <https://doi.org/10.1128/mBio.00551-13>.
- Paulick A, Delalez NJ, Brenzinger S, Steel BC, Berry RM, Armitage JP, Thormann KM. 2015. Dual stator dynamics in the *Shewanella oneidensis* MR-1 flagellar motor. *Mol Microbiol* 96:993–1001. <https://doi.org/10.1111/mmi.12984>.

39. Kearns DB, Losick R. 2003. Swarming motility in undomesticated *Bacillus subtilis*. *Mol Microbiol* 49:581–590. <https://doi.org/10.1046/j.1365-2958.2003.03584.x>.
40. Edwards DH, Errington J. 1997. The *Bacillus subtilis* DivIVA protein targets to the division septum and controls the site specificity of cell division. *Mol Microbiol* 24:905–915. <https://doi.org/10.1046/j.1365-2958.1997.3811764.x>.
41. Stahlberg H, Kutejová E, Muchová K, Gregorini M, Lustig A, Müller SA, Olivieri V, Engel A, Wilkinson AJ, Barák I. 2004. Oligomeric structure of the *Bacillus subtilis* cell division protein DivIVA determined by transmission electron microscopy. *Mol Microbiol* 52:1281–1290. <https://doi.org/10.1111/j.1365-2958.2004.04074.x>.
42. Kloosterman TG, Lenarcic R, Willis CR, Roberts DM, Hamoen LW, Errington J, Wu LJ. 2016. Complex polar machinery required for proper chromosome segregation in vegetative and sporulating cells of *Bacillus subtilis*. *Mol Microbiol* 101:333–350. <https://doi.org/10.1111/mmi.13393>.
43. Hammond LR, White ML, Eswara PJ. 2019. ,vIVA la DivIVA!. *J Bacteriol* 201:e00245-19. <https://doi.org/10.1128/JB.00245-19>.
44. Oliva MA, Halbedel S, Freund SM, Dutow P, Leonard TA, Veprintsev DB, Hamoen LW, Löwe J. 2010. Features critical for membrane binding revealed by DivIVA crystal structure. *EMBO J* 29:1988–2001. <https://doi.org/10.1038/emboj.2010.99>.
45. Levin PA, Kurtser IG, Grossman AD. 1999. Identification and characterization of a negative regulator of FtsZ ring formation in *Bacillus subtilis*. *Proc Natl Acad Sci U S A* 96:9642–9647. <https://doi.org/10.1073/pnas.96.17.9642>.
46. Gardan R, Rapoport G, Débarbouillé M. 1995. Expression of the *rocDEF* operon involved in arginine catabolism in *Bacillus subtilis*. *J Mol Biol* 249:843–856. <https://doi.org/10.1006/jmbi.1995.0342>.
47. Antelmann H, Engelmann S, Schmid R, Hecker M. 1996. General and oxidative stress responses in *Bacillus subtilis*: cloning, expression, and mutation of the alkyl hydroperoxide reductase operon. *J Bacteriol* 178:6571–6578. <https://doi.org/10.1128/jb.178.22.6571-6578.1996>.
48. Bsat N, Chen L, Helmann JD. 1996. Mutation of the *Bacillus subtilis* alkyl hydroperoxide reductase (*ahpCF*) operon reveals compensatory interactions among hydrogen peroxide stress genes. *J Bacteriol* 178:6579–6586. <https://doi.org/10.1128/jb.178.22.6579-6586.1996>.
49. Schönert S, Seitz S, Krafft H, Feuerbaum E-A, Andernach I, Witz G, Dahl MK. 2006. Maltose and maltodextrin utilization by *Bacillus subtilis*. *J Bacteriol* 188:3911–3922. <https://doi.org/10.1128/JB.00213-06>.
50. Murray DS, Chinnam N, Tonthat NK, Whitfill T, Wray LV, Jr, Fisher SH, Schumacher MA. 2013. Structures of the *Bacillus subtilis* glutamine synthetase dodecamer reveal large intersubunit catalytic conformational changes linked to a unique feedback inhibition mechanism. *J Biol Chem* 288:35801–35811. <https://doi.org/10.1074/jbc.M113.519496>.
51. Bendezu OB, Hale CA, Bernhardt TG, de Boer PAJ. 2009. RodZ (YfgA) is required for proper assembly of the MreB actin cytoskeleton and cell shape in *E. coli*. *EMBO J* 28:193–204. <https://doi.org/10.1038/emboj.2008.264>.
52. Gregory JA, Becker EC, Jung J, Tuwatananurak I, Pogliano K. 2010. Transposon Assisted Gene Insertion Technology (TAGIT): a tool for generating fluorescent fusion proteins. *PLoS One* 5:e8731. <https://doi.org/10.1371/journal.pone.0008731>.
53. Gibson DG, Young L, Chuang R-Y, Venter JC, Hutchison CA, Smith HO. 2009. Enzymatic assembly of DNA molecules up to several hundred kilobases. *Nat Methods* 6:343–345. <https://doi.org/10.1038/nmeth.1318>.
54. Ricca E, Cutting S, Losick R. 1992. Characterization of *bofA*, a gene involved in inter-compartmental regulation of pro- σ^k processing during sporulation in *Bacillus subtilis*. *J Bacteriol* 174:3177–3184. <https://doi.org/10.1128/jb.174.10.3177-3184.1992>.
55. Kearns DB, Losick R. 2005. Cell population heterogeneity during growth of *Bacillus subtilis*. *Genes Dev* 19:3083–3094. <https://doi.org/10.1101/gad.1373905>.
56. Yasbin RE, Young FE. 1974. Transduction in *Bacillus subtilis* by Bacteriophage SPP1. *J Virol* 14:1343–1348. <https://doi.org/10.1128/JVI.14.6.1343-1348.1974>.
57. Jaacks KJ, Healy J, Losick R, Grossman AD. 1989. Identification and characterization of genes controlled by the sporulation-regulatory gene *spoOH* in *Bacillus subtilis*. *J Bacteriol* 171:4121–4129. <https://doi.org/10.1128/jb.171.8.4121-4129.1989>.
58. Mirdita M, Ovchinnikov S, Steinegger M. 2021. ColabFold - Making protein folding accessible to all. <https://doi.org/10.1101/2021.08.15.456425>.
59. Jumper J, Evans R, Pritzel A, Green T, Figurnov M, Ronneberger O, Tunyasuvunakool K, Bates R, Židek A, Potapenko A, Bridgland A, Meyer C, Kohl SAA, Ballard AJ, Cowie A, Romera-Paredes B, Nikolov S, Jain R, Adler J, Back T, Petersen S, Reiman D, Clancy E, Zielinski M, Steinegger M, Pacholska M, Berghammer T, Bodenstein S, Silver D, Vinyals O, Senior AW, Kavukcuoglu K, Kohli P, Hassabis D. 2021. Highly accurate protein structure prediction with AlphaFold. *Nature* 596:583–589. <https://doi.org/10.1038/s41586-021-03819-2>.
60. Oliva MA, Trambaiolo D, Löwe J. 2007. Structural insights into the conformational variability of FtsZ. *J Mol Biol* 373:1229–1242. <https://doi.org/10.1016/j.jmb.2007.08.056>.
61. Youngman P, Perkins JB, Losick R. 1984. Construction of a cloning site near one end of Tn917 into which foreign DNA may be inserted without affecting transposition in *Bacillus subtilis* or expression of the transposon-borne *erm* gene. *Plasmid* 12:1–9. [https://doi.org/10.1016/0147-619x\(84\)90061-1](https://doi.org/10.1016/0147-619x(84)90061-1).
62. Hall AN, Subramanian S, Oshiro R, Canzonieri AK, Kearns DB. 2018. SwrD (Ylz) promotes swarming in *Bacillus subtilis* by increasing power to flagellar motors. *J Bacteriol* 200:e00529-17. <https://doi.org/10.1128/JB.00529-17>.